METTL5-mediated m^{6}A modification of 18S rRNA drives oral squamous cell carcinoma progression by enhancing CCND3 translation

LIANLIAN LIU[1*], SURUI SHENG[2*], XIN ZHENG[1*], SHUOJIN HUANG[1], LU WANG[3], DALONG SHU[1], LEILE TANG[4] and QIANTING HE[1]

[1]Department of Oral and Maxillofacial Surgery, The First Affiliated Hospital of Sun Yat-Sen University, Guangzhou, Guangdong 510080, P.R. China; [2]Department of Oral and Maxillofacial-Head and Neck Oncology, Shanghai Ninth People's Hospital, College of Stomatology, Shanghai Jiao Tong University School of Medicine; National Center for Stomatology; National Clinical Research Center for Oral Diseases; Shanghai Key Laboratory of Stomatology, Shanghai 200011, P.R. China; [3]Department of Medical Laboratory, School of Laboratory Medicine and Biotechnology, Southern Medical University, Guangzhou, Guangdong 510515, P.R. China; [4]Department of Cardiovascular Medicine, The Third Affiliated Hospital, Sun Yat-Sen University, Guangzhou, Guangdong 510630, P.R. China

Received June 15, 2025; Accepted December 12, 2025

DOI: 10.3892/ol.2026.15490

Abstract. Oral squamous cell carcinoma (OSCC) is a predominant head and neck malignancy with epigenetic alterations key to its development; however, the role and mechanisms of methyltransferase 5, N6-adenosine (METTL5) in OSCC remain to be elucidated. This study aimed to investigate the functional role and underlying mechanism of METTL5 in OSCC progression. Western blotting analyzed METTL5 expression in OSCC cell lines and tissues, whilst Cell Counting Kit-8, Transwell, colony formation and wound healing assays, as well as cell cycle analysis and nude mouse xenografts were used to assess its functional effects. Moreover, ribosome nascent-chain complex-bound messenger RNA sequencing (RNC-seq) was used to assess gene translation efficiency (TE). Western blotting, Transwell and colony formation assays, and cell cycle analysis were employed for downstream studies. Bioinformatics analyses were conducted to complement mechanistic exploration. The Cancer Genome Atlas data demonstrated that higher METTL5 expression in metastatic head and neck squamous cell carcinoma tissues was significantly associated with poor prognosis. Furthermore, METTL5 knockout significantly inhibited OSCC tumorigenesis and metastasis *in vitro* and *in vivo*. Finally, RNC-seq identified 3,391 genes with reduced TE, with cyclin D3 (CCND3) shown to be a downstream target. In conclusion, METTL5 may promote OSCC progression by regulating CCND3 via N6-methyladenosine-mediated ribosomal methylation, positioning it as a potential therapeutic target in the future.

Introduction

Oral squamous cell carcinoma (OSCC) represents a predominant malignant neoplasm worldwide, accounting for ~90% of oral malignancies and markedly impacting both physiological function and aesthetic appearance. Data from the Global Cancer Observatory (1) indicates that the incidence of OSCC is expected to increase by ~40% by 2040, with a corresponding rise in mortality rates (1). Despite advancements in therapeutic approaches and diagnostic methods, the 5-year overall survival rate of OSCC has shown only modest improvements in recent years, particularly in cases where distant metastasis is detected at diagnosis (2). Moreover, it has been reported that less than 1/2 patients survive >5 years, partly due to the incomplete understanding of the molecular mechanisms underlying the disease and the notable challenge of drug resistance (3).

In the field of oncology, RNA chemical modifications, particularly N6-methyladenosine (m^{6}A) modification, have emerged as key regulators of gene expression dynamics and neoplastic evolution (4,5). These modifications are predominantly identified on messenger RNA (mRNA) and ribosomal RNA (rRNA), and they have notable effects on RNA stability, processing, translation and decay (6,7). Notably, methyltransferase 5,

Correspondence to: Dr Qianting He, Department of Oral and Maxillofacial Surgery, The First Affiliated Hospital of Sun Yat-Sen University, 58 Zhongshan Second Road, Guangzhou, Guangdong 510080, P.R. China
E-mail: heqt3@mail.sysu.edu.cn

Dr Leile Tang, Department of Cardiovascular Medicine, The Third Affiliated Hospital, Sun Yat-Sen University, 600 Tianhe Road, Guangzhou, Guangdong 510630, P.R. China
E-mail: tleil@mail2.sysu.edu.cn

*Contributed equally

Key words: N6-methyladenosine, oral squamous cell carcinoma, methyltransferase 5, N6-adenosine, cyclin D3

N6-adenosine (METTL5) has been identified as a principal m^{6}A-modifying enzyme, responsible for orchestrating m^{6}A modification at the A1832 locus of 18S rRNA. This specific modification serves a key role in ribosomal biogenesis and function, thereby exerting a notable influence on an extensive range of physiological and pathological processes, including the initiation and progression of cancer (8-13).

Preliminary investigations into METTL5 across a spectrum of malignancies have highlighted its complex involvement through several mechanistic pathways (14-16). Notably, a previous study has reported that METTL5/transfer RNA methyltransferase activator subunit 11-2-mediated m^{6}A modification at the A1832 site of 18S rRNA is upregulated in nasopharyngeal carcinoma, fostering tumorigenesis both *in vitro* and *in vivo* (17). Mechanistically, METTL5 contributes to carcinogenesis by promoting the assembly of 80S ribosomes, which in turn enhances the translation of mRNA with a 5'-terminal oligopyrimidine structure. Furthermore, METTL5 enhances the assembly of 80S ribosomes, which in turn activates the transcription of heat shock factor 4b. This process hinders the degradation of mutant p53 protein, thereby promoting nasopharyngeal carcinoma tumorigenesis and contributing to chemotherapy resistance (17). In renal cell carcinoma, increased METTL5 expression is associated with immune dysregulation within the tumor microenvironment. This may influence tumor progression by modulating immune-related pathways, such as the differentiation of T-helper (Th)17 and Th1/Th2 cells, as well as the activity of phosphatidylinositol 3-kinase (18). Furthermore, METTL5 has been identified as a key factor in determining the composition of the tumor microenvironment and the infiltration of immune cells. This is particularly evident in lung adenocarcinoma, where increased METTL5 expression has been associated with unfavorable patient outcomes. The influence of METTL5 in this context is likely due to its ability to modulate immune pathways, which can promote tumor growth and spread by shaping the immune microenvironment (19). Furthermore, in hepatocellular carcinoma, the upregulation of METTL5 has been reported to drive metabolic reprogramming, notably in glucose metabolism pathways, which in turn promotes cancer cell proliferation and metastasis. This metabolic reconfiguration is likely facilitated by the upregulation of key enzymes, including lactate dehydrogenase A, enolase 1, triosephosphate isomerase 1, solute carrier family 2 member 1 and pyruvate kinase M2. Furthermore, METTL5 exerts regulatory control over c-Myc protein stability, which in turn can further modulate tumor cell proliferation (20,21). In breast cancer, augmented METTL5 expression is associated with a more aggressive tumor behavior and reduced survival rates compared with low METTL5 expression. Mechanistically, METTL5 enhances translational capacity and protein synthesis within breast cancer cell lines, thus promoting cancer cell proliferation and survival (22). However, current investigations on the role and mechanistic details of METTL5 in OSCC is still in its early stages. Building upon the pivotal role of METTL5 in diverse types of malignancies, we hypothesize that it may also serve a key role in the pathogenesis and progression of OSCC.

OSCC is a major head and neck malignancy with unclear molecular mechanisms underlying its progression. METTL5 is associated with cancer development, but its role and mechanisms in OSCC remain unknown. The present study aimed to explore the clinical significance of METTL5 in patients with OSCC, its functional role in tumorigenesis and progression, and the underlying molecular mechanisms. The present study analyzed the association of METTL5 with clinical outcomes, conducted *in vitro/in vivo* experiments to assess its impact on OSCC cell proliferation, metastasis and tumor growth, and used RNA-seq and bioinformatics to identify its regulated pathways and targets. The present study aims to fill the knowledge gap of METTL5 in OSCC and lay a theoretical foundation for potential therapeutic target discovery.

Materials and methods

Patient samples. All clinical samples used in the present study were collected from The First Affiliated Hospital of Sun Yat-sen University (Guangzhou, China). Prior to sample collection, written informed consent was obtained from all the patients. All patient-related studies were reviewed and approved by the Independent Ethics Committee for Clinical Research and Animal Trials of The First Affiliated Hospital of Sun Yat-sen University [approval no. (2022)229], and performed in accordance with the Declaration of Helsinki. Inclusion criteria for the present study were as follows: i) Pathologically confirmed primary OSCC; ii) no neoadjuvant therapy; iii) complete clinical/follow-up data; and iv) an age of ≥18 years with normal liver/kidney function. Exclusion criteria were as follows: i) Secondary OSCC/synchronous malignancies; ii) history of other cancer types (5 years); iii) severe systemic diseases; and iv) incomplete data. Samples (n=4) were collected from August to October 2022. Table SI presents the demographic information and tumor characteristics of patients in the present study.

Cell culture and lentiviral transduction/transfection. The HSC3 cell line was purchased from the Japanese Collection of Research Bioresources Cell Bank (cat. no. JCRB0623). SCC15 cells were purchased from the American Type Culture Collection (cat. no. CRL-1623). The Human Oral Keratinocytes (HOK) cell line was purchased from ScienCell Research Laboratories, Inc. (cat. no. 2610). Cells were maintained in a humidified incubator with 5% CO_2 at 37˚C and cultured in DMEM/F-12 medium (cat. no. C11330500BT) supplemented with 1% penicillin/streptomycin (cat. no. 15140-122; Gibco; Thermo Fisher Scientific, Inc.) and 10% FBS(Gibco; Thermo Fisher Scientific, Inc.).

Both METTL5 knockout and overexpression systems were constructed for functional assays: Knockout system (lentivirus-mediated): The fourth-generation CRISPR plasmid system was used, including packaging plasmids (TAT, RAII, HEMP2 and VSVG) and target plasmids (LentiCRISPRv2 [negative control, NC group], lentiCRISPRv2-METTL5-human-sg1, lentiCRISPRv2-METTL5-human-sg2 [target groups]; purchased from Guangzhou IGE Biotechnology Co., Ltd.]). The interim cell line for lentiviral packaging was 293T cells (purchased from the American Type Culture Collection), which were used to produce viral particles.

Overexpression system (transient transfection): The overexpression plasmid (pFLAG-CMV2-METTL5/pFLAG-CMV2-CCND3; overexpression, OE) and empty vector

(pFLAG-CMV2; negative control, NC) were purchased from Guangzhou IGE Biotechnology Co., Ltd.), and introduced into cells via transient transfection (no lentiviral packaging required).

Lentiviral transfection (for knockout) was performed as follows: $1x10^6$ 293T cells were seeded in T25 flasks 1 day prior to transfection at 37˚C and cultured until reaching 60% confluence. The transfection mixture was prepared by combining the packaging plasmids (0.5 μg TAT, 0.5 μg RAII, 0.5 μg HEMP2, 0.5 μg VSVG) and target plasmids (2 μg per construct) with 200 μl Opti-MEM medium (Gibco; Thermo Fisher Scientific, Inc.). Separately, Lipofectamine 2000 (Invitrogen; Thermo Fisher Scientific, Inc.) was gently mixed with 200 μl Opti-MEM and incubated at room temperature for 5 min. The plasmid mixture and Lipofectamine 2000 solution were then combined, gently mixed, and incubated at room temperature for 20 min (plasmid: Lipofectamine 2000 ratio=3.5 μg: 7 μl). The complete medium of 293T cells was aspirated and replaced with 5 ml antibiotic-free DMEM containing 10% FBS, followed by the addition of the entire plasmid-Lipofectamine 2000 complex. Cells were incubated at 37˚C in a 5% CO_2 incubator for 12-24 h before medium replacement.

Lentiviral particles were collected every 24 h for 2-3 consecutive days. The collected medium was centrifuged at ~450 x g (2,000 rpm) for 5 min at 4˚C, and the viral supernatant was aliquoted into sterile 1.5 ml EP tubes and stored at -80˚C. For infection of target OSCC cells (HSC3 and SCC15), cells were seeded in T25 flasks and cultured until 60% confluence. Lentiviral particles were added at a multiplicity of infection (MOI) of 10 along with polybrene (final concentration: 8 μg/ml) to enhance transduction efficiency. Cells were incubated at 37˚C in a 5% CO_2 incubator for 24-48 h.

Following transduction, the selection method was antibiotic selection using puromycin; the selection concentration was 2.5-3 μg/ml, and the maintenance concentration was 1.0-1.5 μg/ml. Cells were cultured for >48 h until all untransfected cells died. After selection, cells were maintained in medium containing the maintenance concentration of puromycin. The transduced cells were then passaged, and protein extraction was performed for western blot analysis to verify the gene knockout efficiency of METTL5. The time interval between transduction and subsequent experimentation was 48-72 h after successful transduction and selection.

Transient transfection (for METTL5 overexpression): OSCC cells (HSC3 and SCC15) were seeded in 6-well plates and cultured until 60% confluence. The transfection mixture was prepared by combining 4 μg of pFLAG-CMV2-METTL5/pFLAG-CMV2-CCND3 (or pFLAG-CMV2) with 250 μl Opti-MEM medium, then mixed with 5 μl Lipofectamine 2000 (incubated at room temperature for 20 min). The mixture was added to cells in antibiotic-free medium, and cells were incubated at 37˚C for 48 h. The time interval between transfection and subsequent experimentation was 48 h. Western blot analysis was performed to verify the METTL5 overexpression level.

CCND3 overexpression in METTL5-depleted HSC3 cells: METTL5-depleted HSC3 cells (sgMETTL5 HSC3 cells) were seeded in 6-well plates and cultured until 60% confluence. The CCND3 overexpression plasmid (pFLAG-CMV2-CCND3) and empty vector (pFLAG-CMV2; negative control) were introduced via transient transfection: 4 μg of plasmid (or empty vector) was mixed with 250 μl Opti-MEM medium, followed by 5 μl Lipofectamine 2000. The mixture was incubated at room temperature for 20 min, then added to cells in antibiotic-free medium. Cells were incubated at 37˚C (5% CO_2) for 48 h. The time interval between transfection and subsequent experimentation was 48 h. Western blot analysis was performed to verify CCND3 overexpression efficiency before subsequent functional assays. The sgRNA sequences used in the present study are listed in Table SII.

Immunohistochemistry (IHC) staining. Tissues from the mouse model were first fixed in 4% paraformaldehyde (PFA) (w/v in phosphate-buffered saline, PBS) at 4˚C for 24 h. Fixed tissues were embedded in paraffin resin, and serial sections were cut into 4 μm-thick slices using a microtome. For dewaxing and rehydration, sections were processed through a descending alcohol series: xylene (twice for 10 min each), 100% ethanol (twice for 5 min each), 95% ethanol (5 min), 80% ethanol (5 min), 70% ethanol (5 min), and finally rinsed with distilled water for 5 min. Antigen retrieval was performed by immersing sections in 0.01 M citrate buffer (pH 6.0) and heating in a microwave oven at 95-100˚C for 15 min. After natural cooling to room temperature, sections were washed with PBS (3 times for 5 min each).

To block endogenous peroxidase activity, sections were treated with 3% hydrogen peroxide at room temperature for 10 min, followed by three washes with PBS (5 min each). Non-specific binding sites were blocked using 5% BSA (w/v in PBS; cat. no. 4240GR100; Saiguo Biotechnology Co., Ltd.) at room temperature for 30 min. Subsequently, sections were incubated overnight with primary antibodies at 4˚C: Anti-Ki-67 and anti-METTL5. After three washes with PBS (5 min each), sections were incubated with a horseradish peroxidase (HRP)-conjugated goat anti-rabbit secondary antibody at room temperature for 60 min. Details of all primary and secondary antibodies are in Table SIII.

Immunoreactivity was visualized using a DAB detection kit (cat. no. GK6007; Beijing Genetech Co., Ltd.) as the chromogen substrate. Sections were incubated with DAB working solution at room temperature for 3-5 min (monitoring staining intensity under a light microscope to avoid over-staining). The reaction was terminated by rinsing with distilled water. Sections were then counterstained with hematoxylin at room temperature for 2 min, differentiated with 1% hydrochloric acid in ethanol for 30 sec, and dehydrated through an ascending alcohol series (70, 80, 95 and 100% ethanol for 5 min each) followed by xylene (twice for 10 min each). Finally, sections were mounted with neutral gum and a coverslip was applied.

Stained sections were imaged using a Leica inverted light microscope (Leica Microsystems) at magnifications of 400x; scale bar, 50 μm. IHC scoring was performed based on a semi-quantitative immunoreactivity scoring system (4). Briefly, the proportion of positive staining cells was scored as follows: 0 (absent), 1 (<10%), 2 (10-50%), and 3 (>50%). Staining intensity was scored as: 0 (negative), 1 (weak), 2 (moderate), and 3 (strong). The final IHC score was calculated by multiplying the percentage score by the intensity score, resulting in a range of 0-9. Image analysis and scoring were performed using ImageJ software (Version 1.53; National Institutes of Health).

Western blotting. Total protein was extracted from OSCC cells (HSC3/SCC15), HOK and human tissues using RIPA buffer (cat. no. C1053; Applygen Technologies, Inc.). Protein concentration was determined via the BCA protein assay kit (cat. no. P0012; Beyotime Biotechnology) following the manufacturer's instructions.

Equal amounts of protein (20 μg per lane) were loaded onto 10% SDS-PAGE gels for separation, then transferred onto a PVDF membrane (cat. no. IPVH00010; Merck KGaA). The membrane was blocked with 5% non-fat skimmed milk (dissolved in TBS-Tween; TBST) for 2 h at room temperature; TBST buffer contained 0.1% Tween-20 (v/v) in Tris-buffered saline.

Subsequently, the membrane was incubated with primary antibodies (listed in Table SIII) at 4˚C overnight. After three washes with TBST (10 min each), the membrane was incubated with species-matched secondary antibodies (HRP-conjugated) at room temperature for 1 h.

Protein bands were detected using a super-sensitive ECL kit (cat. no. P0018FS; Beyotime Biotechnology). The membrane was incubated with the ECL working solution (1:1 mixture of reagent A and B) for 5 min at room temperature, then visualized using the Tanon 5200 Multi Intelligent Imaging System (Tanon Science and Technology Co., Ltd.). Band intensities were quantified using ImageJ software (Version 1.53; National Institutes of Health) for densitometric analysis.

Cell Counting Kit-8 (CCK-8). Cell viability was monitored using a CCK-8 kit (cat. no. CK04; Dojindo Laboratories, Inc.). A total of 1x10^3 cells (HSC3 or SCC15) per well were plated onto 96-well plates and cultured in DMEM/F-12 with 1% FBS. CCK-8 working solution was then applied to the cells for 2 h, according to the manufacturer's instructions. A microplate reader (cat. no. A51119500C; Thermo Fisher Scientific, Inc.) was then used to measure the absorbance of the supernatant at 450 nm.

Cell colony formation assay. HSC3 and SCC15 cells were seeded in 6-well plates at a density of 1x10^3 cells/well without additional drug treatment. Cells were incubated in a humidified incubator with 5% CO_2 at 37˚C for 2 weeks to allow colony formation. After the incubation period, cells were washed twice with PBS (5 min each wash). Subsequently, cells were fixed with 4% formaldehyde at room temperature for 15 min. The fixative was discarded, and cells were stained with 0.1% crystal violet solution (w/v in distilled water) at room temperature for 20 min. Excess crystal violet was rinsed off with distilled water, and the plates were air-dried. A colony was defined as a cluster containing ≥50 cells. Colony quantification was performed using ImageJ software (Version 1.53; National Institutes of Health). Briefly, images of stained wells were captured by camera (cat. no. ILCE-7M4, Sony Corporation), and the ImageJ software (Version 1.53; National Institutes of Health) was used to count the number of discrete colonies based on color thresholding and size gating.

Transwell assay. Transwell migration assays were performed using Transwell chambers with an 8 μm pore size (cat. no. 353097; Falcon®; Corning Life Sciences). No Matrigel was used in the assay, confirming this as a migration experiment. The lower chamber of the 24-well Transwell system was filled with DMEM supplemented with 10% FBS. HSC3 and SCC15 cells were resuspended in serum-free DMEM, and 5x10^4 cells/well were seeded into the upper chamber in a total volume of 200 μl. Cells were incubated in a humidified incubator with 5% CO_2 at 37˚C for 48 h to allow migration through the pores.

After incubation, non-migrated cells on the upper surface of the membrane were gently removed with a cotton swab. Migrated cells adhering to the lower surface were fixed with 4% formaldehyde at room temperature for 30 min, then stained with 0.1% crystal violet solution at room temperature for 30 min. Excess stain was rinsed off with PBS, and the membranes were air-dried. Migrated cells were observed and counted using a Leica inverted light microscope (Leica Microsystems) at a magnification of 100x. Scale bar, 100 μm were included in the figure legends for reference. Three random fields were selected per membrane to count migrated cells, and the average number was calculated for statistical analysis.

Wound healing assay. A total of 2x10^5 HSC3 and SCC15 cells were seeded into each well of a 6-well plate. The cells were cultured in DMEM/F-12 medium supplemented with 10% FBS (Gibco; Thermo Fisher Scientific, Inc.) without additional drug treatment, and no serum starvation was performed before the assay. When cell confluence reached ~90% of the plate surface, a sterile 200 μl pipette tip was used to scratch a straight wound across each well. The scratched cells were gently washed away with PBS (twice) to remove cell debris, and fresh DMEM/F-12 medium containing 10% FBS was added to each well. Wound width was measured at 0 h and the endpoint time (8, 12 or 24 h) under the bright field of a Leica inverted light microscope (Leica Microsystems). The percentage of wound healing was calculated using the formula: Wound healing (%)=1-(width$_t$/width$_0$) x100, where width$_0$ is the initial wound width at 0 h and width$_t$ is the wound width at the endpoint time.

Cell cycle analysis. Cell cycle progression of HSC3 and SCC15 cells was assessed using a Cell Cycle Kit (cat. no. CCS012; MultiSciences (Lianke) Biotech Co., Ltd.) (no cytokines/chemokines used). 2x10^5-1x10^6 harvested cells were washed with PBS, then mixed with 1 ml DNA staining solution + 10 μl permeabilization solution (kit components), vortexed 5-10 sec, and incubated at room temperature in the dark for 30 min. Stained cells were analyzed on a BD FACSCanto™ II flow cytometer (low injection speed), and data (G0/G1, S, G2/M phases) were processed via FlowJo v10.8.1 (BD Biosciences). No antibodies were used.

Xenograft mouse model. A total of 12 6-week-old female BALB/c nude mice (18-22 g) were purchased from the Animal Experiment Center of The First Affiliated Hospital, Sun Yat-Sen University. Mice were housed under specific pathogen-free conditions (20-25˚C; relative humidity, 40-70%; 12 h light/12 h dark cycle and ad libitum access to sterile food and water).

1x10^6 tumor cells (METTL5 knockout and control SCC15 cells, in 50 μl sterile PBS) were subcutaneously injected into the right dorsal flank of nude mice. Palpable tumors were monitored once weekly. Humane endpoints: Excess tumor

size (maximum permitted size was 20 mm), >20% weight loss, poor mobility or distress.

Experiment ended 18 days post-injection. Mice were euthanized by cervical dislocation, and death confirmed by 5-min absence of breathing/heartbeat. Tumors were excised, weighed, measured and imaged. IHC samples were fixed with 4% paraformaldehyde at 4˚C for 24 h.

All experiments were approved by the Ethical Committee of The First Affiliated Hospital, Sun Yat-Sen University [approval no. (2024)051] and conducted per institutional guidelines.

Ribosome nascent-chain (RNC) complex-bound mRNA sequencing (mRNA-seq). To examine the alteration of mRNA translation after METTL5 depletion, mRNA-seq was performed on total mRNAs and RNC-mRNAs from METTL5-knocked-out or control HSC3 cells. RNC-mRNAs were extracted as previously described. Cells were quickly washed with ice-cold PBS containing 100 mg/ml cycloheximide and then collected and lysed in 1.2 ml lysis buffer containing 1% Triton X-100 in ribosome buffer [which contains 20 mM HEPESKOH (pH 7.4), 15 mM MgCl2, 200 mM KCl, 100 mg/ml cycloheximide and 2 mM dithiothreitol] for 30 min on ice. Cell lysates were centrifuged at 16,200 x g for 10 min at 4˚C to remove the cell debris. The supernatants were transferred on the surface of 12 ml of ribosome buffer containing 30% sucrose. RNC-mRNAs were pelleted after ultra-centrifugation at 185,000 x g for 5 h at 4˚C. RNAs in total cell lysates and RNC-mRNAs were extracted with TRIzol® reagent (cat. no. 15596018; Thermo Fisher Scientific, Inc.) and subjected to RNA-sequencing (RNA-seq).

For RNA-seq experiments, the following details were followed: i) RNA sample preparation kit: TRIzol® reagent (cat. no. 15596018; Thermo Fisher Scientific, Inc.); ii) sample quality/integrity verification: RNA quality was assessed by Q20 (>90%), Q30 (>85%) values, and RNA integrity number (RIN) ≥7.0 using a Microplate Reader (Molecular Devices, Gemini XPS) and Qubit® 4 Fluorometer (cat. no. Q33216, Thermo Fisher Scientific, Inc.); iii) sequencing type: Paired-end sequencing (PE150) on the DNBSEQ platform; iv) sequencing kit: DNBSEQ-T7RS High-throughput Sequencing Kit (cat. no. 940-000268-00; Shenzhen BGI Genomics Co., Ltd.); v) Final library loading concentration: 2 nM, measured by reverse transcription-quantitative PCR (qPCR) using the Qubit® ssDNA Assay Kit (cat. no. Q10212, Invitrogen; Thermo Fisher Scientific, Inc.) for molar concentration quantification; vi) Data analysis software: SOAPnuke (version 1.5.6; https://github.com/BGI-flexlab/SOAPnuke) for raw data filtering, HISAT2 (version 2.1.0; https://daehwankimlab.github.io/hisat2/) for genome alignment, Bowtie2 (version 2.3.4.3; http://bowtie-bio.sourceforge.net/bowtie2/index.shtml) for gene alignment, RSEM (version 1.2.28; https://deweylab.github.io/RSEM/) for gene expression quantification, DESeq2 (version 1.40.2; https://bioconductor.org/packages/3.16/bioc/html/DESeq2.html) for differential expression analysis.

The TE was calculated using the following formula: TE=transcripts per million (TPM) in RNC-seq/TPM in input RNA-seq. Genes with a TE ratio of sgMETTL5 (sgM5)/NC <0.667 and >1.5 were classified as decreased TE (TE down) and enhanced TE (TE up), respectively.

Gene Ontology (GO) and pathway analyses. GO and pathway analyses of TE-down mRNAs identified in RNC-seq data were performed using the Bioinformatics Webtool (https://www.bioinformatics.com.cn/), and significantly enriched pathways were identified.

Datasets. Gene Expression Profiling Interactive Analysis (GEPIA) database (http://gepia.cancer-pku.cn/): The dataset 'TCGA-HNSC' (The Cancer Genome Atlas Head and Neck Squamous Cell Carcinoma) was queried with the search term 'METTL5' to analyze METTL5 mRNA expression levels in tumor vs. normal tissues. Survival analysis was performed via GEPIA using the 'TCGA-HNSC' dataset with METTL5 expression stratified into 'low' and 'high' groups (median cutoff). University of Alabama at Birmingham Cancer data analysis Portal (UALCAN; https://ualcan.path.uab.edu/index.html): The dataset 'TCGA-HNSC' was queried with the search term 'METTL5' to analyze the association between METTL5 expression and clinical parameters (lymph node metastasis, cancer stage, tumor grade).

Statistical analysis. Quantitative data are presented as mean ± standard deviation. Unpaired two-tailed Student's t-test was used to assess statistically significant differences between two experimental groups, while one-way ANOVA followed by Tukey's honest significant difference post hoc test was applied for multiple groups. For non-parametric data, the Kruskal-Wallis test was used, with Dunn's post hoc test for pairwise comparisons following a significant result. Pearson's correlation analysis was performed for the data presented in Fig. S4C (from GEPIA2; http://gepia2.cancer-pku.cn/). All experiments were performed with three independent biological repeats. Statistical significance was defined as $P<0.05$; for differential gene analysis (where applicable), the significance cut-off levels were set as adjusted $P<0.05$ and $|\log2 \text{ fold change}|>1$. Statistical analyses were performed using GraphPad Prism (version 8.0; Dotmatics). $^{*}P<0.05$, $^{**}P<0.01$; $^{***}P<0.001$; $^{****}P<0.0001$.

Results

METTL5 expression is elevated in head and neck squamous cell carcinoma (HNSCC) and is associated with poor prognosis of HNSCC. To ascertain whether METTL5 contributes to cancer progression, the present study performed an analysis of METTL5 mRNA levels in HNSCC using the Gene Expression Profiling Interactive Analysis database (http://gepia.cancer-pku.cn/, dataset are provided in Methods section: Datasets). The findings indicated that METTL5 expression was significantly higher in tumor tissues compared with that in normal tissues (Fig. 1A). In addition, data from University of Alabama at Birmingham Cancer data analysis Portal (https://ualcan.path.uab.edu/index.html, dataset are provided in Methods section: Datasets) revealed that elevated METTL5 expression was significantly associated with increased lymph node metastasis (vs. no lymph node metastasis), advanced cancer stages (vs. early stages) and higher tumor grades (vs. lower grades) in HNSCC (Fig. 1C-E). Furthermore, patients with higher METTL5 expression exhibited significantly worse overall survival than those with low METTL5 expression

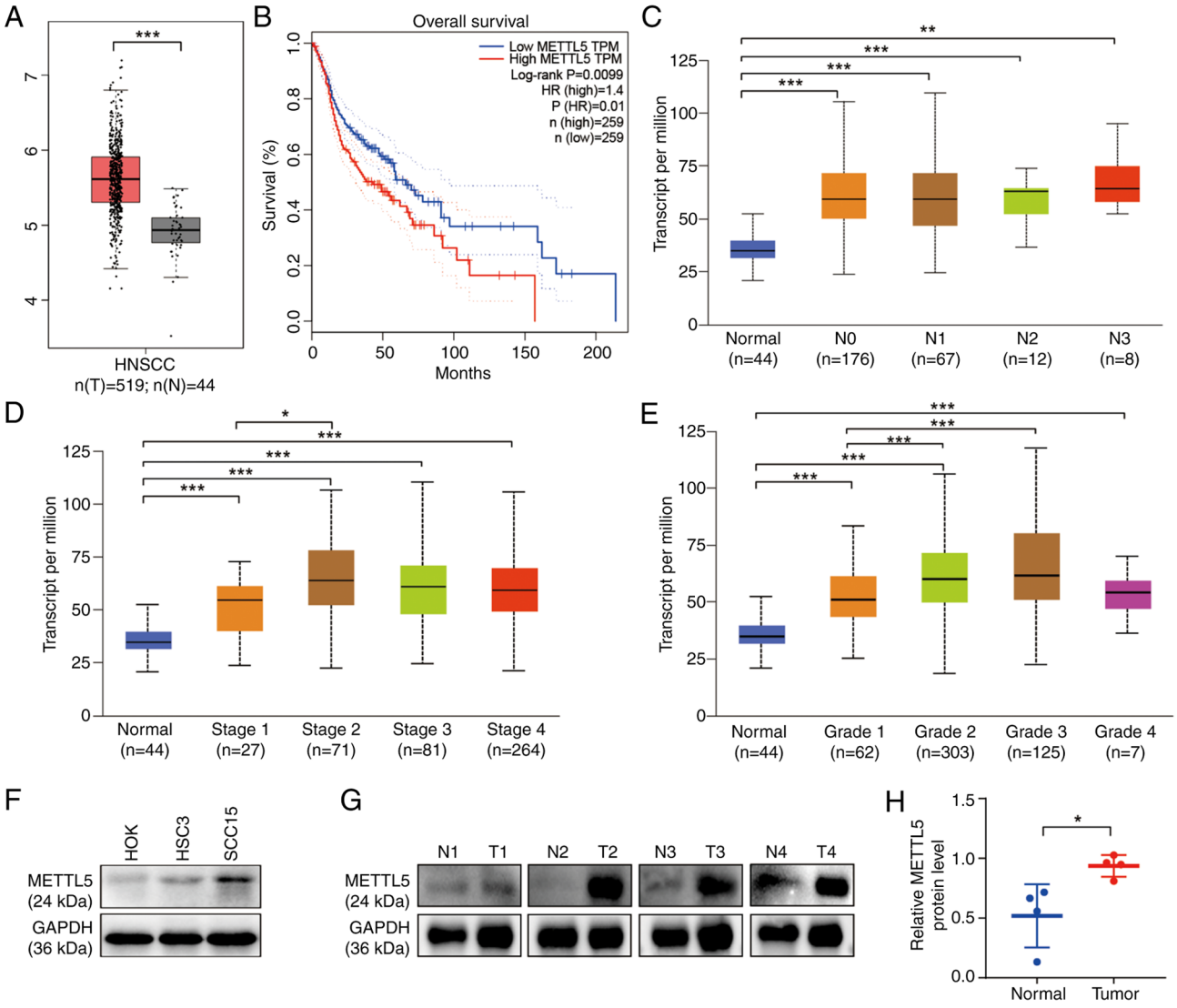

Figure 1. METTL5 is elevated in HNSCC and is associated with poor prognosis of HNSCC. (A) Comparison of mRNA levels of METTL5 in HNSCC with normal tissues in TCGA-HNSCC dataset. (B) Overall survival of patients between METTL5-high (n=259) and METTL5-low (n=259) groups. (C) METTL5 expression level in normal and HNSCC tissues with different stages of lymph node metastasis. (D) METTL5 expression level in normal tissues and different stages of HNSCC tissues. (E) METTL5 expression level in normal HNSCC tissues and different grades of HNSCC tissues. (F) METTL5 protein level in OSCC(HSC3, SCC15) and HOK cell lines. (G) Representative bands of METTL5 protein expression levels in human OSCC and paired normal tissues measured by western blotting. (H) Semi-quantification of METTL5 protein expression levels in human OSCC and paired normal tissues. *P<0.05, **P<0.01; ***P<0.001. METTL5, methyltransferase 5, N6-adenosine; HNSCC, head and neck squamous cell carcinoma; TCGA, The Cancer Genome Atlas; OSCC, oral squamous cell carcinoma; HOK, human normal oral epithelial keratinocyte; HR, hazard ratio; TPM, transcripts per million; N, normal; T, tumor.

(Fig. 1B). Collectively, these findings suggest that METTL5 is key to regulating the progression of HNSCC.

Furthermore, western blotting analysis was used to assess METTL5 expression in two OSCC cell lines and a human normal oral epithelial keratinocyte (HOK) cell line. The results revealed that OSCC cells exhibited markedly higher METTL5 expression compared with that in HOK cells (Fig. 1F). Furthermore, western blotting analysis demonstrated significantly elevated METTL5 protein levels in human OSCC tissues compared with that in normal tissues (Fig. 1G and H).

Knockout of METTL5 inhibits the progression of OSCC in vitro. To elucidate the function of METTL5 in OSCC, the present study established stable knockout cell lines using SCC15 and HSC3 cells, targeting METTL5 with independent sgMETTL5 (Figs. 2A and S1A). Notably, the METTL5 knockout cells demonstrated a significant decrease in proliferative capacity (Figs. 2B and S1B) and a colony formation (Figs. 2C and S1C) compared with that in the control group. Furthermore, the Transwell migration and wound healing assays indicated that METTL5 knockout significantly impaired the migration of OSCC cells *in vitro* compared with that in control cells (Figs. 2D, E, S1D and E).

Overexpression of METTL5 promotes the progression of OSCC. A METTL5 overexpression system was also constructed using lentivirus to investigate the functional impact of METTL5 in OSCC (Figs. 3A and S2A). The findings revealed that METTL5 overexpression led to a significant increase in cellular proliferation (Figs. 3B and S2B) and colony formation (Fig. 3D) in OSCC cells. Furthermore, the

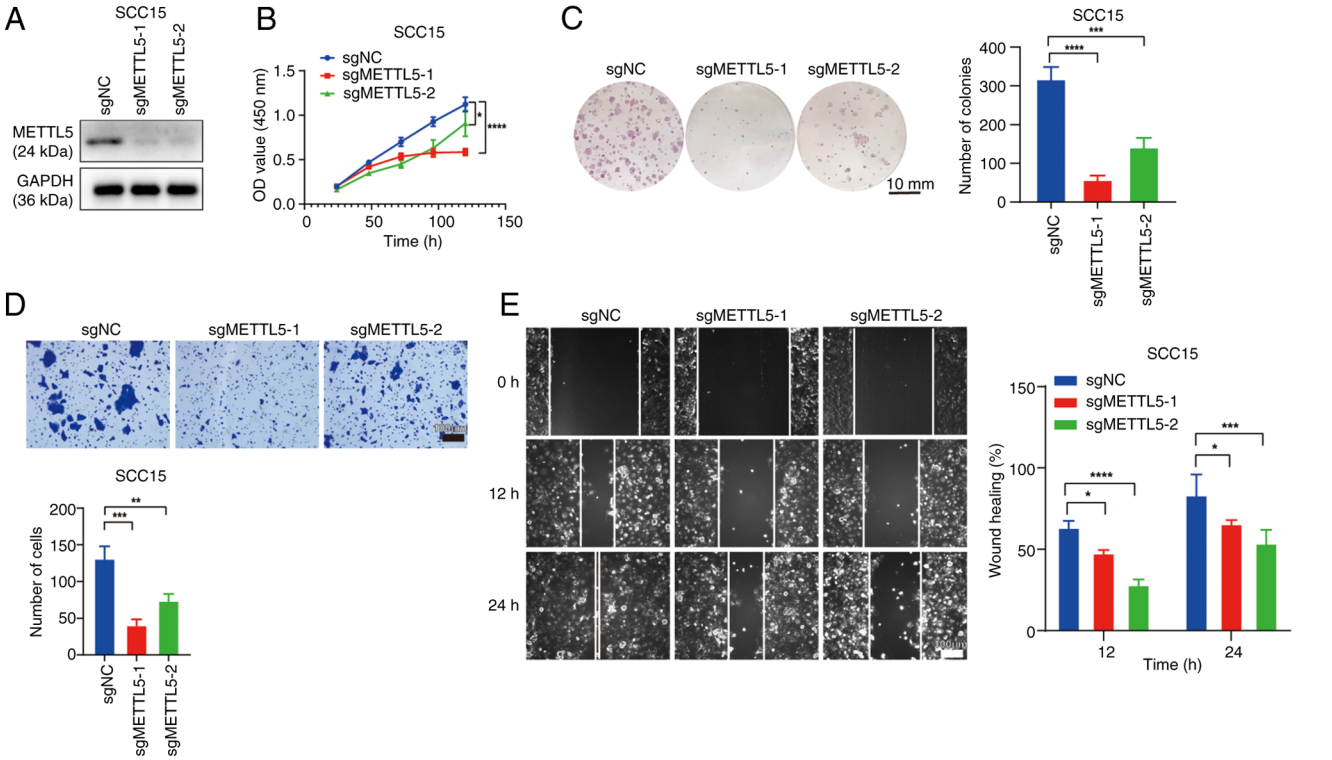

Figure 2. Knockout of METTL5 inhibits the progression of OSCC *in vitro*. (A) Validation of METTL5 stable knockout in SCC15 cells by western blotting. Results of (B) Cell Counting Kit-8 assay, (C) colony formation assay, (D) Transwell assay and (E) wound healing assay after knockout of METTL5 in SCC15 cells. *P<0.05, **P<0.01; ***P<0.001; ****P<0.0001. METTL5, methyltransferase 5, N6-adenosine; NC, negative control; OSCC, oral squamous cell carcinoma; sg, small guide RNA; NC, negative control; OD, optical density.

overexpression of METTL5 enhanced the migration of OSCC cells (Figs. 3C and S2C), indicating a role for METTL5 in promoting the malignancy of OSCC.

Inhibition of METTL5 suppresses tumor growth in vivo. Xenograft tumor-formation assays were subsequently performed to assess the role of METTL5 in the regulation of OSCC tumorigenesis *in vivo*. METTL5 knockout and control SCC15 cells were inoculated subcutaneously into the right dorsal flank of nude mice, with tumor volumes monitored throughout the experiment. The results indicated that the subcutaneous tumors were notably larger in the control group compared with that in the sgMETTL5 group (Fig. 4A). Compared with that in the control group, the growth curve of the xenograft tumor and the final tumor weights further demonstrated that the knockout of METTL5 significantly impeded tumor growth *in vivo* (Fig. 4B and C). Moreover, IHC analysis revealed that the expression level of METTL5 was significantly diminished in xenograft tumors derived from the sgMETTL5 group compared with that in the control group (Fig. 4D and E). In addition, xenograft tumors from the sgMETTL5 groups exhibited significantly lower Ki-67 expression compared with that in the control group, indicating that METTL5-knockout xenograft tumors were potentially less malignant (Fig. 4D and E).

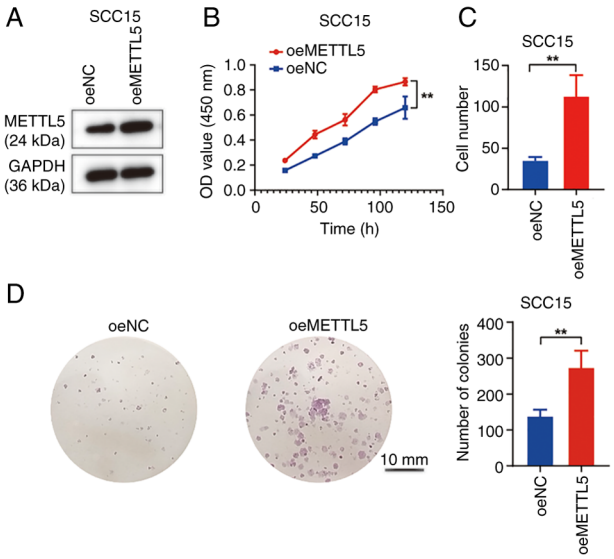

Figure 3. Overexpression of METTL5 promotes the progression of OSCC. (A) Validation of METTL5 overexpression in SCC15 cells by western blotting. (B) Results of the Cell Counting Kit-8 assay after METTL5 overexpression in SCC15 cells. (C) Statistical results of the Transwell assay after METTL5 overexpression in SCC15 cells. (D) Results of the colony formation assay after knockout of METTL5 in SCC15 cells. **P<0.01. METTL5, methyltransferase 5, N6-adenosine; OSCC, oral squamous cell carcinoma; oe, overexpression; NC, negative control; OD, optical density.

Knockout of METTL5 selectively inhibits the translation of oncogenic mRNAs. The present study further utilized RNC-mRNA-seq to assess mRNA translation profiles in METTL5-depleted and control cells. The RNC-mRNA-seq analysis revealed 3,391 genes with TE-down and 1,020 genes with TE-up in METTL5-depleted OSCC cells (Fig. 5A). This suggests that METTL5-knockout predominantly leads

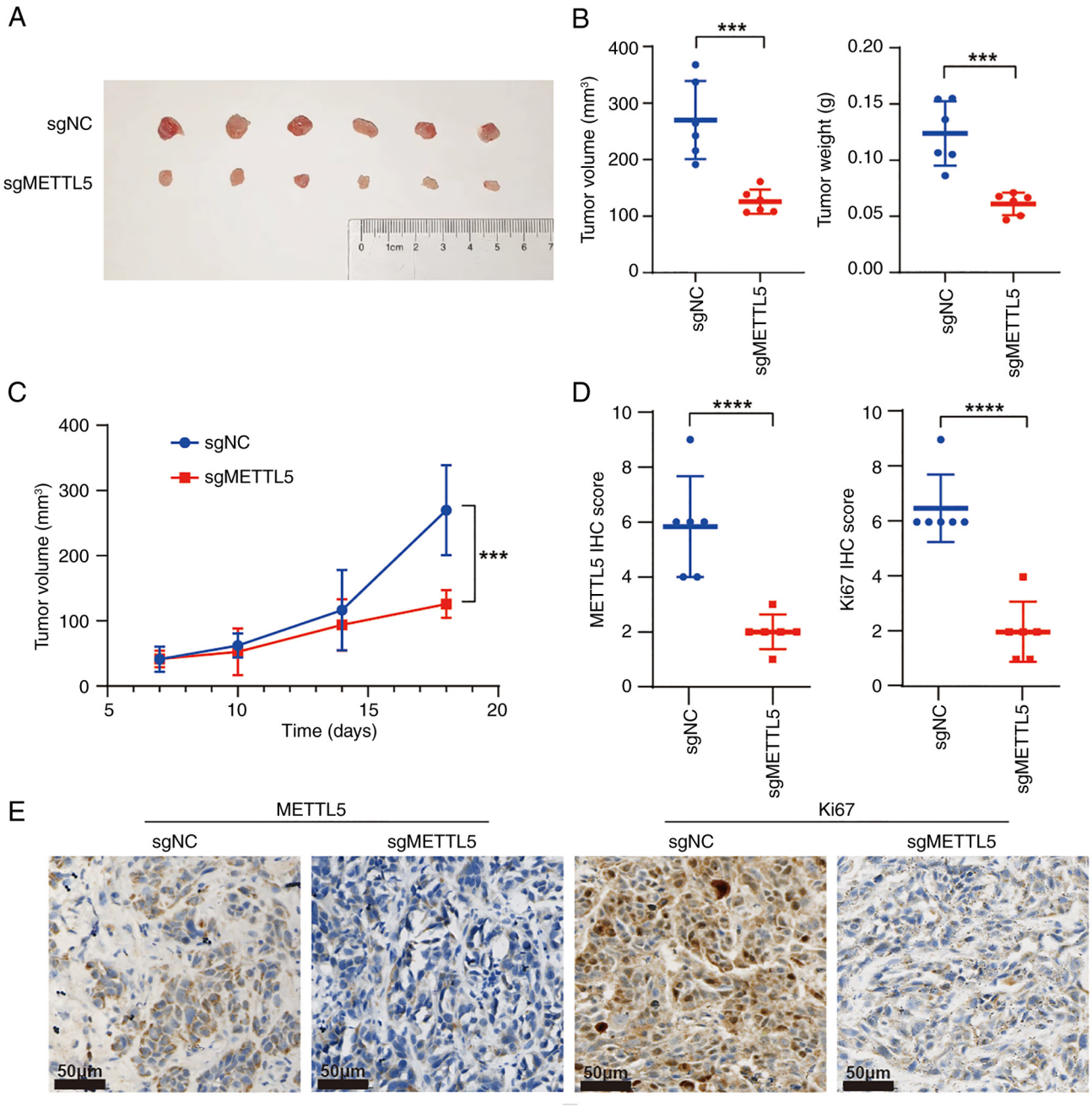

Figure 4. Inhibition of METTL5 suppresses tumor growth *in vivo*. (A) Representative images of subcutaneous tumors from the SCC15 cell mouse model. (B) Quantification of tumor weight and tumor volume. (C) Tumor volume changes during treatment. (D) Quantitative analysis of IHC scores for METTL5 and Ki-67 expression. (E) Representative images of METTL5 and Ki-67 staining. **P<0.01; ***P<0.001. METTL5, methyltransferase 5, N6-adenosine; sg, small guide RNA; NC, negative control; IHC, immunohistochemistry.

to a decrease in TE rather than an increase. Furthermore, GO analysis of genes with TE-down revealed that 'Cell cycle'-related processes were significantly enriched (Fig. 5B). Among the cell cycle-related TE-down genes identified, the present study prioritized cyclin D3 (CCND3) as it is a well-characterized cyclin driving cell cycle phase transition, and its dysregulation is directly associated with tumor growth (20). Subsequently, western blotting demonstrated that the levels of the cell-cycle regulator CCND3 were markedly decreased in sgMETTL5 cells compared with that in control cells (Fig. 5C). Consistent with this, cell cycle assays revealed that knockout of METTL5 induced the proportion of OSCC cells in the G_0/G_1 phase and decreased the proportion in the G_2/M phase (Fig. 6D and S3). In summary, the results indicate that the depletion of METTL5 in OSCC cells significantly alters the translational profile. This alteration not only results in a general decrease in TE but also specifically impacts the translation of certain mRNAs, particularly those associated involved in cell cycle regulation.

CCND3 overexpression partially rescues cancer cell phenotypes in METTL5-depleted OSCC cells. The aforementioned results indicate that the downregulation of METTL5 expression disrupts the translation process, particularly for mRNAs involved in the 'Cell cycle' pathway. Consequently, rescue experiments (Fig. 6) were performed using HSC3

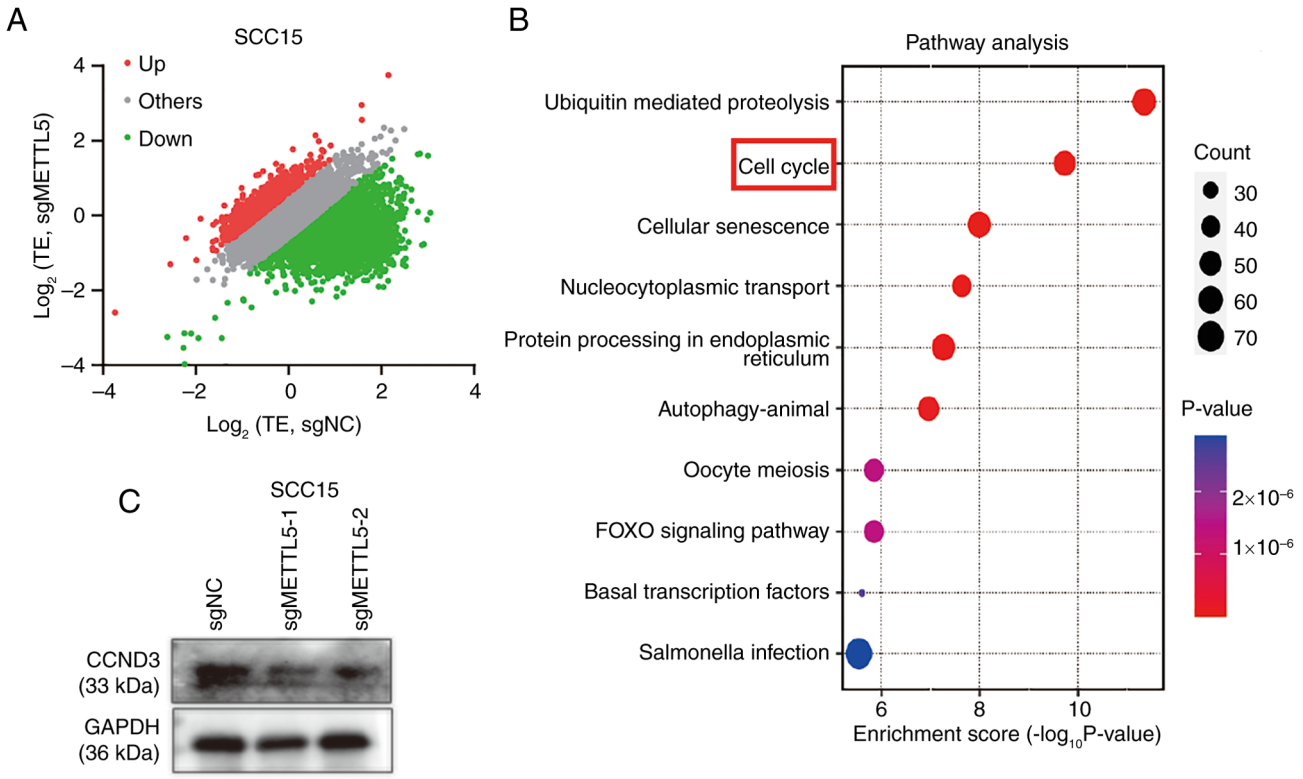

Figure 5. Knockout of METTL5 selectively inhibits the translation of oncogenic mRNAs. (A) TE scatter plot of METTL5 knockout and control SCC15 cells. (B) Pathway enrichment of TE-downregulated genes. (C) Western blotting confirmed the decreased protein levels of CCND3 in METTL5 knockout SCC15 cells. METTL5, methyltransferase 5, N6-adenosine; TE, translation efficiency; CCND3, cyclin D3; sg, small guide RNA; NC, negative control.

cells due to their notably increased TE and higher baseline invasion capacity, which are key to robustly evaluate the functional recovery of migration ability. Although SCC15 cells demonstrated higher basal METTL5 expression (Fig. 1F), the characteristics of HSC3 made it a more suitable model for validating the rescue effect of CCND3 overexpression. Therefore, the present study overexpressed CCND3 in METTL5-depleted HSC3 cells (Fig. 6A). The results revealed that overexpression of CCND3 partially rescued the migration and colony formation capacity of METTL5-depleted OSCC cells (Fig. 6B and C). Moreover, for cell cycle analysis, METTL5 knockout induced a cell cycle arrest in the G_0/G_1 phase compared with that in control cells, and CCND3 overexpression reversed this (Figs. 6D and S3). Collectively, the results suggest that METTL5-mediated m^{6}A modification contributes to translational dysregulation, potentially influencing OSCC progression. To explore the potential broader relevance of the findings of the present study, the expression patterns of METTL5 and CCND3 were analyzed across several cancer types using TCGA data. The results demonstrated that METTL5 (Fig. S4A) and CCND3 (Fig. S4B) exhibited differential expression in multiple cancer types compared with that in adjacent normal tissues. Moreover, although there is no existing literature reporting a direct association between METTL5 and CCND3 in other cancer types, to the best of our knowledge, the weak but statistically significant mRNA-level correlation demonstrated in the generated scatter plot indicates that METTL5 transcription minimally drives CCND3 mRNA expression (Fig. S4C).

Discussion

Ribosomes are intricate macromolecular machines that serve as the cellular catalysts for protein synthesis. They are key to translating all cellular proteins and eukaryotic cytoplasmic ribosomes, and are intricately assembled from four types of rRNA and ~80 distinct ribosomal proteins. Universally, they are organized into two subunits, each consisting of a complex array of proteins and several rRNAs (23). rRNAs are the architects of the ribosomal subunits, shaping both their form and function, and they provide the enzymatic activity key to protein synthesis. Emerging evidence indicates that rRNAs may influence multiple aspects of protein synthesis, including the recruitment of mRNA, modulation of TE for specific mRNAs and the facilitation of ribosomal shunting (24,25). rRNAs are distinguished as one of the most extensively modified class of RNAs, with ~2% of their nucleotides subject to post-transcriptional modifications. These modifications constitute a notable source of ribosome diversity and are increasingly acknowledged for their role in ribosome specialization. There is extensive research that implicates abnormalities in the enzymes responsible for rRNA modification, as well as variations in the extent of these modifications, in the etiology of developmental disorders, genetic conditions and cancer (24).

rRNA constitutes >80% of the total RNA in the cell (26), yet the physiological functions of rRNA modifications remain to be elucidated. m^{6}A modification refers to the reversible process of methylation on the 6th nitrogen atom of RNA adenine catalyzed by methyltransferase (27). The m^{6}A methylation mark is also present within the decoding center of

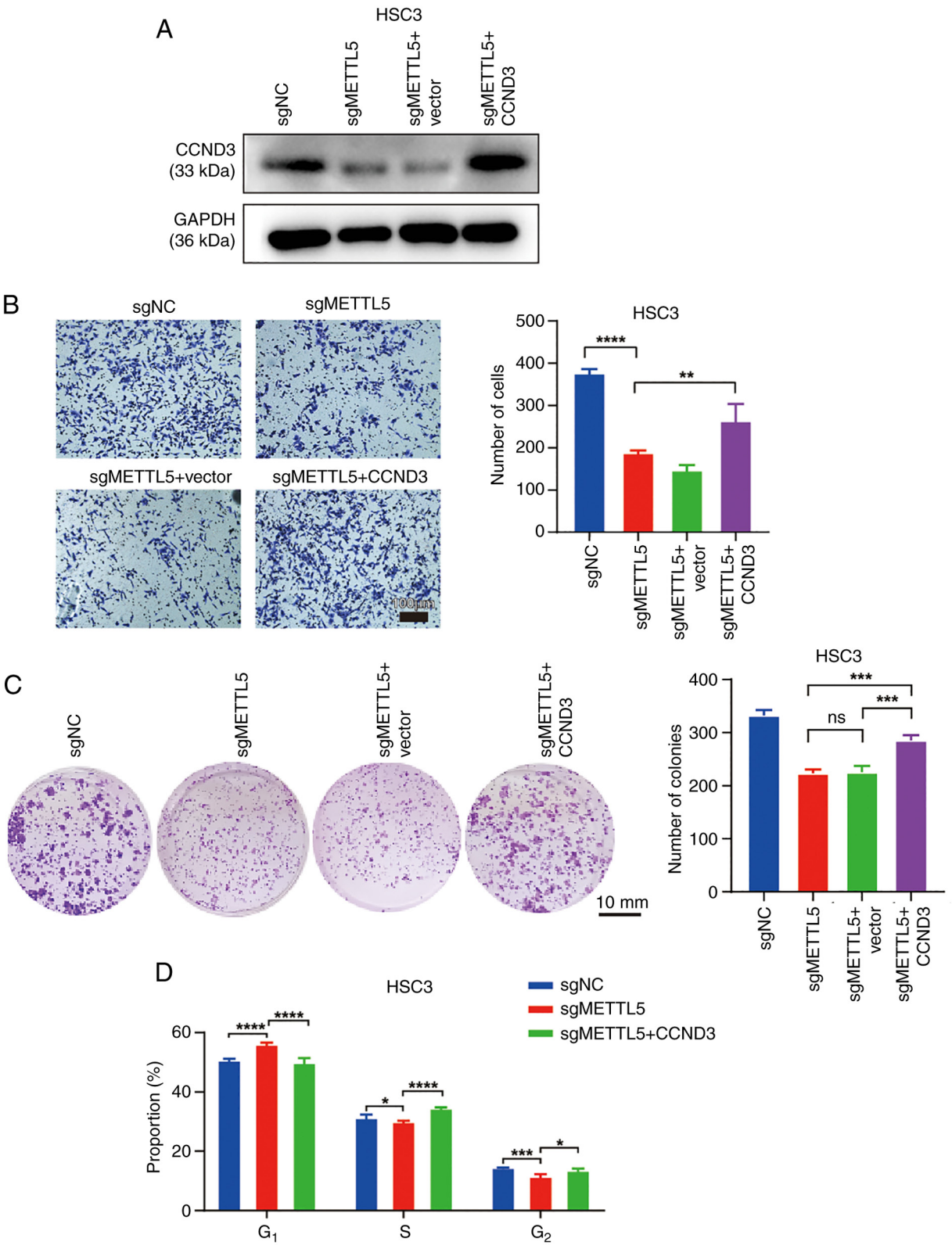

Figure 6. CCND3 overexpression partially rescues cancer cell phenotype in METTL5-depleted oral squamous cell carcinoma cells. (A) Validation of CCND3 overexpression in METTL5-depleted HSC3 cells. Results of the (B) Transwell, (C) colony formation and (D) cell cycle assays after CCND3 overexpression in METTL5-depleted HSC3 cells. *P<0.05, **P<0.01; ***P<0.001; ****P<0.0001. METTL5, methyltransferase 5, N6-adenosine; CCND3, cyclin D3; sg, small guide RNA; NC, negative control; ns, not significant.

18S rRNA (28); however, the specific biological function of m^{6}A on 18S rRNA remains to be elucidated. METTL5, an enzyme responsible for the m^{6}A modification of rRNA, has been associated with several types of cancer, including breast cancer, liver cancer and nasopharyngeal carcinoma. Moreover, the role of METTL5 in catalyzing m^{6}A modifications appears to differ across distinct cancer types, such as breast cancer (promoting cell growth) and nasopharyngeal carcinoma

(enhancing chemoresistance) (17,22,29). Research suggests that METTL5-mediated m^{6}A modifications are associated with intracellular TE (30), tumor cell proliferation, cell pluripotency (10) and stress response (31). However, the specific role and mechanism of METTL5 in OSCC remain to be fully elucidated.

The present study identified that the m^{6}A methyltransferase METTL5 is significantly overexpressed in OSCC and is associated with a poor patient prognosis. The results also demonstrated that downregulation of METTL5 significantly reduced the proliferative and migratory capacities of human OSCC cells, whilst its overexpression promoted OSCC progression *in vitro*. Furthermore, the *in vivo* OSCC models in the present study utilizing METTL5-deficient SCC15 cells, corroborated the role of METTL5 in the development and progression of OSCC within a living organism. At the molecular level, the present study identified the CCND3 signaling pathway as a key m^{6}A-modified target that mediates the effects of METTL5 on OSCC progression. Collectively, the results of the present study, including both *in vitro* and *in vivo* experiments, provide evidence highlighting the notable role of the m^{6}A modification in regulating OSCC tumorigenesis and its progression. Although METTL5 depletion phenocopies translational disruption, meaning that METTL5 knockout leads to phenotypes (such as reduced translation efficiency) similar to those caused by direct disruption of translational machinery, direct causality requires further validation to confirm m^{6}A-dependent mechanisms.

Emerging evidence has revealed the oncogenic functions of CCND3 in regulating the progression of several diseases, including cancer. In diffuse large B-cell lymphoma, it has been reported that pathways associated with cell cycle and DNA replication are markedly upregulated in patients harboring mutations in the CCND3 gene (32). MicroRNA-4779 has been reported to suppress cancer cell proliferation by inducing cell cycle arrest and apoptosis through the direct targeting of p21 (RAC1) activated kinase 2 and CCND3. Furthermore, the downregulation of CCND3 has been shown to induce cell cycle arrest and apoptosis (33). In addition, polypyrimidine tract-binding protein 1 has been identified to enhance the translation of CCND3 by binding to the 5'-untranslated region of the CCND3 mRNA, thereby facilitating cell cycle progression and tumor growth (23). Therefore, targeting the CCND3 represents a promising therapeutic strategy for cancer treatment. Moreover, METTL5-mediated rRNA m^{6}A modification is known to modulate overall translation activity and the selective translation of certain mRNAs (31). The results of the present study demonstrated that CCND3 mRNA was affected by METTL5 expression, and that knockout of METTL5 diminished CCND3 protein levels. This indicates that METTL5-mediated m^{6}A modification regulates the TE of CCND3 mRNA. Furthermore, the present study revealed that the forced activation of CCND3 restored the migration capacity of METTL5 knockout cells. This finding suggests that METTL5-mediated m^{6}A deposition is a predominant, although not exclusive, regulator of CCND3 translation.

Notably, the HSC3 and SCC15 cell lines used in the present study are derived from tongue squamous cell carcinoma, with HSC3 from lymph node metastasis (34). Due to the heterogeneity of OSCC across oral subsites, the findings of the present study may not fully represent OSCC from other sites, which warrants validation in more diverse cell lines and samples. Furthermore, he limitations in evaluating the role of METTL5 in OSCC invasion and metastasis are acknowledged. The *in vivo* experiments in the present study were restricted to subcutaneous xenografts, which do not fully recapitulate the oral mucosal microenvironment, including epithelial-mesenchymal interactions and immune cell infiltration. This lack of microenvironment-relevant models limits the clinical translatability of the findings, as the effects of METTL5 cannot be definitively associated with the context-specific mechanisms driving invasion and metastasis in native oral tissues. Moreover, the potential involvement of METTL5 in OSCC metastasis is supported by *in vitro* migration data and the results indicating that high METTL5 expression is associated with lymph node metastasis and poor prognosis rather than direct *in vivo* evidence. Future studies utilizing orthotopic models or patient-derived xenografts with intact microenvironments will be key to validate these associations and clarify the role of METTL5 in clinically relevant invasion and metastasis processes.

Furthermore, although the present study demonstrated the promotional role of METTL5 in OSCC progression through a series of *in vitro* and *in vivo* experiments, and revealed its potential function in regulating the TE of CCND3, certain limitations should be acknowledged. Notably, the present study did not directly verify whether the m^{6}A modification level at the A1832 site of 18S rRNA was indeed reduced after METTL5 knockout. Due to the current unavailability of commercial site-specific m^{6}A antibodies targeting the A1832 site of 18S rRNA, and the technical challenges in conventional m^{6}A-quantitive (q) PCR and associated techniques to resolve adjacent modification sites in rRNA, the present study could not obtained direct experimental evidence regarding the changes in modification levels at this specific site. Therefore, the mechanism by which METTL5 selectively regulates the TE of specific mRNAs (particularly CCND3) by catalyzing m^{6}A modification at the A1832 site of 18S rRNA currently remains a hypothesis based on existing research findings and known mechanisms in associated fields. In future studies, with the development of specific detection technologies, further verification of the dynamic changes of this modification site under METTL5 regulation using methods such as m^{6}A-qPCR and m^{6}A-cross-linking and immunoprecipitation/RNA immunoprecipitation-qPCR targeting the A1832 site of 18S rRNA should be performed to further clarify this molecular mechanism. However, due to the conserved functions of METTL5 in regulating translation and the extensive involvement of CCND3 in cell cycle control across malignancies, future studies should explore whether such an axis exists in other cancer types, which could further expand the translational significance of this regulatory relationship.

Additionally, the functional validation of CCND3 as a downstream mediator of METTL5 in the present study was limited to *in vitro* assays, and the absence of *in vivo* rescue experiments (for example, overexpressing CCND3 in METTL5-knockout xenografts) prevents the definitive establishment of the extent to which CCND3 mediates the pro-tumorigenic effects of METTL5 *in vivo*. This suggests that

other translationally downregulated genes may also contribute markedly to OSCC progression downstream of METTL5.

In conclusion, an elevated expression level of METTL5 in patients with OSCC is associated with an unfavorable prognosis. Moreover, the downregulation of METTL5 expression through is associated with a decrease in m^{6}A rRNA methylation and a selective decrease in the TE of oncogene CCND3 in OSCC. These findings indicate the potential inhibitory effect of METTL5 knockout on OSCC tumorigenesis and progression in both *in vitro* and *in vivo* settings. The results of the present study contribute to furthering the understanding of the epigenetic network that governs OSCC progression. However, although the results demonstrate the prognostic value of METTL5, its potential as a therapeutic target requires further validation in future studies. METTL5 is anticipated to offer potential novel biomarkers and therapeutic targets for the diagnosis and treatment of OSCC in the future.

Acknowledgements

Not applicable.

Funding

The present study was funded by the National Natural Science Foundation of China (grant no. 82002871), Natural Science Foundation of Guangdong Province (grant no. 2023A1515220258) and Foundation and Application Foundation Project in Guangzhou (grant no. SL2023A04J02127).

Availability of data and materials

The data generated in the present study may be found in the China National Center for Bioinformation (CNCB) under accession number OMIX012047 or at the following URL: https://share.cncb.ac.cn/AZg3Lt9OjY/OMIX012047/. The remaining data generated in the present study may be requested from the corresponding author.

Authors' contributions

LL performed the experiments and drafted the manuscript. LL and XZ confirm the authenticity of all the raw data. SS and XZ performed the experiments and acquired the data. SH participated in the analysis of the data. LW, DS, LT and QH designed the present study. LT and QH supervised the present study and revised the manuscript. All authors read and approved the final manuscript.

Ethics approval and consent to participate

Human data and samples were obtained with written informed consent and the use was approved by the Independent Ethics Committee for Clinical Research and Animal Trials of The First Affiliated Hospital of Sun Yat-Sen University [approval no. (2022)229]. The nude mouse experiments performed were approved by the Independent Ethics Committee for Clinical Research and Animal Trials of The First Affiliated Hospital of Sun Yat-Sen University [approval no. (2024)051].

Patient consent for publication

Not applicable.

Competing interests

The authors declare that they have no competing interests.

References

1. Tan Y, Wang Z, Xu M, Li B, Huang Z, Qin S, Nice EC, Tang J and Huang C: Oral squamous cell carcinomas: State of the field and emerging directions. Int J Oral Sci 15: 44, 2023.
2. Hedberg ML, Goh G, Chiosea SI, Bauman JE, Freilino ML, Zeng Y, Wang L, Diergaarde BB, Gooding WE, Lui VW, *et al*: Genetic landscape of metastatic and recurrent head and neck squamous cell carcinoma. J Clin Invest 126: 169-180, 2016.
3. Lo Nigro C, Denaro N, Merlotti A and Merlano M: Head and neck cancer: Improving outcomes with a multidisciplinary approach. Cancer Manag Res 9: 363-371, 2017.
4. Han H, Yang C, Zhang S, Cheng M, Guo S, Zhu Y, Ma J, Liang Y, Wang L, Zheng S, *et al*: METTL3-mediated m^{6}A mRNA modification promotes esophageal cancer initiation and progression via Notch signaling pathway. Mol Ther Nucleic Acids 26: 333-346, 2021.
5. Chen Z, Chen J, Xu X, Li Q, Zhang C, Li S, Liu L, Cao C, Chen D and He Q: METTL3-mediated ALDH m^{6}A methylation regulates the malignant behavior of BMI1$^+$ HNSCC stem cells. Oral Dis 30: 1061-1071, 2024.
6. Pan L, She H, Wang K, Xia W, Tang H, Fan Y and Ye J: Characterization of the m^{6}A regulator-mediated methylation modification patterns in oral squamous cell carcinoma. Sci Rep 13: 6617, 2023.
7. Qin Z, Bai J, He H and Li B: Expression and significance of m^{6}A-RNA-methylation in oral cancer and precancerous lesion. Front Oncol 13: 1013054, 2023.
8. Li H, Wu H, Wang Q, Ning S, Xu S and Pang D: Dual effects of N^6-methyladenosine on cancer progression and immunotherapy. Mol Ther Nucleic Acids 24: 25-39, 2021.
9. Qi YN, Liu Z, Hong LL, Li P and Ling ZQ: Methyltransferase-like proteins in cancer biology and potential therapeutic targeting. J Hematol Oncol 16: 89, 2023.
10. Xing M, Liu Q, Mao C, Zeng H, Zhang X, Zhao S, Chen L, Liu M, Shen B, Guo X, *et al*: The 18S rRNA m^6 A methyltransferase METTL5 promotes mouse embryonic stem cell differentiation. EMBO Rep 21: e49863, 2020.
11. Ignatova VV, Stolz P, Kaiser S, Gustafsson TH, Lastres PR, Sanz-Moreno A, Cho YL, Amarie OV, Aguilar-Pimentel A, Klein-Rodewald T, *et al*: The rRNA m^{6}A methyltransferase METTL5 is involved in pluripotency and developmental programs. Genes Dev 34: 715-729, 2020.
12. Wang L, Liang Y, Lin R, Xiong Q, Yu P, Ma J, Cheng M, Han H, Wang X, Wang G, *et al*: Mettl5 mediated 18S rRNA N6-methyladenosine (m^{6}A) modification controls stem cell fate determination and neural function. Genes Dis 9: 268-274, 2022.
13. Liu X, Ma H, Ma L, Li K and Kang Y: The potential role of methyltransferase-like 5 in deficient mismatch repair of uterine corpus endometrial carcinoma. Bioengineered 13: 5525-5536, 2022.
14. Wang Z, Liu J, Yang Y, Xing C, Jing J and Yuan Y: Expression and prognostic potential of ribosome 18S RNA m^{6}A methyltransferase METTL5 in gastric cancer. Cancer Cell Int 21: 569, 2021.
15. Shinde H and Kadam US: Growing prospects of RNA therapeutics: A case of METTL5 and 18S rRNA m^{6}A modification. Mol Ther 32: 11-12, 2024.
16. van Tran N, Ernst FGM, Hawley BR, Zorbas C, Ulryck N, Hackert P, Bohnsack KE, Bohnsack MT, Jaffrey SR, Graille M and Lafontaine DLJ: The human 18S rRNA m^{6}A methyltransferase METTL5 is stabilized by TRMT112. Nucleic Acids Res 47: 7719-7733, 2019.
17. Chen B, Huang Y, He S, Yu P, Wu L and Peng H: N^6-methyladenosine modification in 18S rRNA promotes tumorigenesis and chemoresistance via HSF4b/HSP90B1/mutant p53 axis. Cell Chem Biol 30: 144-158.e10, 2023.

18. Wei Z, Chen Y, Zeng Z, Peng Y, Li L, Hu N, Gao X, Cai W, Yin L, Xu Y, *et al*: The novel m6A writer METTL5 as prognostic biomarker probably associating with the regulation of immune microenvironment in kidney cancer. Heliyon 8: e12078, 2022.
19. Sun S, Fei K, Zhang G, Wang J, Yang Y, Guo W, Yang Z, Wang J, Xue Q, Gao Y and He J: Construction and comprehensive analyses of a METTL5-associated prognostic signature with immune implication in lung adenocarcinomas. Front Genet 11: 617174, 2020.
20. Xia P, Zhang H, Lu H, Xu K, Jiang X, Jiang Y, Gongye X, Chen Z, Liu J, Chen X, *et al*: METTL5 stabilizes c-Myc by facilitating USP5 translation to reprogram glucose metabolism and promote hepatocellular carcinoma progression. Cancer Commun (Lond) 43: 338-364, 2023.
21. Wang L and Peng JL: METTL5 serves as a diagnostic and prognostic biomarker in hepatocellular carcinoma by influencing the immune microenvironment. Sci Rep 13: 10755, 2023.
22. Rong B, Zhang Q, Wan J, Xing S, Dai R, Li Y, Cai J, Xie J, Song Y, Chen J, *et al*: Ribosome 18S m^6A Methyltransferase METTL5 promotes translation initiation and breast cancer cell growth. Cell Rep 33: 108544, 2020.
23. Kang H, Heo S, Shin JJ, Ji E, Tak H, Ahn S, Lee KJ, Lee EK and Kim W: A miR-194/PTBP1/CCND3 axis regulates tumor growth in human hepatocellular carcinoma. J Pathol 249: 395-408, 2019.
24. Sloan KE, Warda AS, Sharma S, Entian KD, Lafontaine DLJ and Bohnsack MT: Tuning the ribosome: The influence of rRNA modification on eukaryotic ribosome biogenesis and function. RNA Biol 14: 1138-1152, 2017.
25. Burman LG and Mauro VP: Analysis of rRNA processing and translation in mammalian cells using a synthetic 18S rRNA expression system. Nucleic Acids Res 40: 8085-8098, 2012.
26. Noller HF: Ribosomal RNA and translation. Annu Rev Biochem 60: 191-227, 1991.
27. Tian S, Lai J, Yu T, Li Q and Chen Q: Regulation of gene expression associated with the N6-Methyladenosine (m6A) enzyme system and its significance in cancer. Front Oncol 10: 623634, 2021.
28. Sepich-Poore C, Zheng Z, Schmitt E, Wen K, Zhang ZS, Cui XL, Dai Q, Zhu AC, Zhang L, Sanchez Castillo A, *et al*: The METTL5-TRMT112 N^6-methyladenosine methyltransferase complex regulates mRNA translation via 18S rRNA methylation. J Biol Chem 298: 101590, 2022.
29. Peng H, Chen B, Wei W, Guo S, Han H, Yang C, Ma J, Wang L, Peng S, Kuang M and Lin S: N^6-methyladenosine (m^6A) in 18S rRNA promotes fatty acid metabolism and oncogenic transformation. Nat Metab 4: 1041-1054, 2022.
30. Dai Z, Zhu W, Hou Y, Zhang X, Ren X, Lei K, Liao J, Liu H, Chen Z, Peng S, *et al*: METTL5-mediated 18S rRNA m^6A modification promotes oncogenic mRNA translation and intrahepatic cholangiocarcinoma progression. Mol Ther 31: 3225-3242, 2023.
31. Lei K, Lin S and Yuan Q: N^6-methyladenosine (m^6A) modification of ribosomal RNAs (rRNAs): Critical roles in mRNA translation and diseases. Genes Dis 10: 126-134, 2023.
32. Hua W, Li Y, Yin H, Du KX, Zhang XY, Wu JZ, Liang JH, Shen HR, Gao R, Li JY, *et al*: Analysis of CCND3 mutations in diffuse large B-cell lymphoma. Ann Hematol 103: 5729-5739, 2024.
33. Koo KH and Kwon H: MicroRNA miR-4779 suppresses tumor growth by inducing apoptosis and cell cycle arrest through direct targeting of PAK2 and CCND3. Cell Death Dis 9: 77, 2018.
34. Ribeiro IP, Rodrigues JM, Mascarenhas A, Kosyakova N, Caramelo F, Liehr T, Melo JB and Carreira IM: Cytogenetic, genomic, and epigenetic characterization of the HSC-3 tongue cell line with lymph node metastasis. J Oral Sci 60: 70-81, 2018.